www.editada.org

International Journal of Combinatorial Optimization Problems and Informatics, 17(3), 2026, 302-316. ISSN: 2007-1558.
https://doi.org/10.61467/2007.1558.2026.v17i3.1251

EMG Hand-Gesture Classification Using Time, Frequency and Time–Frequency Domain Features with Machine-Learning Techniques

José Manuel López-Villagómez[1,2], Ruth Ivonne Mata-Chávez[1], Juan Manuel López-Hernández[1], Jorge Manuel Barrios-Sánchez[1,3], Miguel Alfonso López-Alonso[2], José Manuel Moreno-Loera[1], Alberto Nicolas Moreno[1]

[1] Universidad de Guanajuato.
[2] Universidad Virtual del Estado de Guanajuato.
[3] Universidad Rafael Nuñez.
Email address(es): jm.lopezvillagomez@ugto.mx, ruth@ugto.mx, jmlopez@ugto.mx, jm.barriossanchez@ugto.mx, miglopez@uveg.edu.mx, jm.morenoloera@ugto.mx, an.lopezmoreno@ugto.mx.
✉Corresponding author: José Manuel López-Villagómez

Abstract. This paper investigates single-channel surface electromyography for seven hand gestures using a compact feature-based machine-learning pipeline. EMG from twelve participants was segmented into contraction-level windows and described by time-, frequency- and time–frequency-domain features, complemented with simple feature-engineering transformations. Support vector machines with linear, RBF and polynomial kernels and a multilayer perceptron were evaluated. First, models were trained on the full feature set, obtaining a no-PCA baseline where linear and polynomial SVM achieved accuracies slightly above ninety-two percent and the neural network reached about eighty-nine percent. Then, Principal Component Analysis was applied, retaining two, five, nine and twelve components. Very low dimensionality degraded all models, whereas retaining nine to twelve components slightly improved RBF SVM and clearly benefited the neural network, which reached almost ninety-four percent accuracy.

Keywords: EMG, Hand-gesture classification, Feature extraction SVM,ANN, PCA.

Article information
Received: Nov 27, 2025
Accepted: Jan 28, 2026

1 Introduction

Substantial disability is produced by upper-limb loss, restricting the performance of activities of daily living (Unanyan & Belov, 2021). Partial restoration of function has been pursued with myoelectric prostheses, in which robotic arms or hands are controlled using residual muscle signals (Chen et al., 2023). Electromyographic (EMG) signals are used to capture the electrical activity generated by muscles during contraction and relaxation. EMG amplitudes are typically measured within the 0–100 mV range, and the motor-neuron drive that activates the musculature is generally regarded as stochastic, yielding EMG with inherently stochastic characteristics (Zheng et al., 2022). The EMG spectrum typically spans approximately 20–500 Hz, with most spectral energy concentrated around 50–150 Hz. Intuitive prosthetic-hand control is enabled by accurately inferring which finger or combination of fingers, is intended for activation to execute a given gesture (Li et al., 2022). However, because different gestures recruit partially overlapping myoelectric patterns, the decoding of individual movements from EMG is rendered intrinsically difficult. Reliable discrimination is typically achieved through appropriate signal conditioning and feature extraction, together with dimensionality reduction (e.g., PCA) and supervised classification using models such as SVM and ANN (Chen et al., 2023). Raw EMG signals are typically preprocessed through filtering and rectification, after which features are extracted. The resulting descriptors are commonly grouped into three families: time-domain, frequency-domain, and time–frequency-domain features (Sharma et al., 2024). Research evidence has shown that time-domain and time–frequency representations often yield superior performance for EMG analysis relative to using frequency-domain features alone. Feature vectors may subsequently be compacted via principal component analysis prior to classification (Khan et al., 2021).

Consequently, a broad range of techniques has been explored for EMG pattern identification. Feature extraction was coupled with bagging and boosting ensemble classifiers for hand-movement recognition (Subasi & Qaisar, 2022). Time-domain descriptors, such as maximum amplitude and average maximum amplitude, were proposed and used to recognize and classify finger-related muscular activity, time-domain analysis is often preferred due to its comparatively low computational burden (Lv et al., 2023). An approach to improve the classification of twelve finger movements was proposed in (Anam et al., 2021), employing k-nearest neighbor (k-NN) with two cross-validation protocols, K-fold and stratified K-fold. In (Tepe & Demir, 2022), the performance of support vector machines for EMG classification was investigated under both offline (non-real-time) and real-time conditions. The authors in (Narayan, 2021), the classification of surface EMG (sEMG) signals using support vector machines and naïve Bayes was compared for the identification of six distinct hand movements. The discrete wavelet transform (DWT) was applied to denoise the signals and to extract time–frequency domain (TFD) features. A composite feature vector was then constructed, integrating both TFD and time-domain (TD) descriptors.

Machine-learning and deep-learning methods introduced in recent years have complemented established approaches for EMG-signal classification and have been reported to improve performance in several settings. In (Rasnayake et al., 2022), EMG analysis based on the wavelet transform and artificial neural networks was investigated with the aim of developing an assistive system for individuals with disabilities. In (Lee et al., 2021), classifiers for individual finger gestures were developed from electromyographic recordings using machine-learning methods under fixed electrode placement. EMG data were acquired from ten participants performing ten hand and finger gestures, including seven single-finger gestures. Time-domain features were computed and used to train gesture-specific models based on artificial neural networks, support vector machines, random forests, and logistic regression. An alternative study proposed a weighted ensemble framework that integrates transfer learning across six pre-trained CNNs (DenseNet121, Xception, EfficientNetB2, ResNet-50, MobileNetV2, VGG16) for stroke classification on 2,376 brain MR images. The three best individual models (98.0–98.4% validation accuracy) were combined using Dirichlet-weighted averaging, yielding 99.84% test accuracy and exceeding previously reported baselines. These results suggest that ensemble learning can enhance diagnostic performance in small medical datasets (Alhatemi & Savas, 2024).

Deep-learning models for brain-tumor classification in MRI (e.g., CNNs, ResNet) were reviewed across studies from 2010 to 2022. High performance was frequently reported for detection and segmentation; however, many methods depend on large, well-curated datasets and clinical uptake remains limited. The review underscored the value of optimized preprocessing procedures and hybrid (e.g., ensemble or multi-stage) frameworks to strengthen diagnostic reliability in brain-tumor management (Joshi & Singh, 2024). An accuracy of 94.94% was achieved on single-channel EMG data by the proposed model, indicating its capacity to discriminate among complex grasp patterns (Coskun et al., 2022). In this study (Sun et al., 2022), a multi-scale feature extraction network (MSFEnet) based on channel–spatial attention was introduced for EMG classification. Temporal and multi-scale convolutions, together with attention modules, were employed to capture salient channel- and spatial-domain features. The approach was evaluated on the NinaPro DB2 and CapgMyo DB-a datasets, achieving gesture-recognition accuracies of up to 98.85%. A clinical decision support system was developed and assessed across ten machine-learning classifiers using expert-weighted synthetic data for typhoid-fever diagnosis and grading. Ensembles based on random forests and decision trees attained 87% accuracy, exceeding the average clinician performance (71%), by encoding diagnostic logic as probabilistic yes/no decisions. These findings suggest that interpretable tree-based models are viable for real-time infectious-disease applications, while persistent issues of generalization, data noise, and interoperability remain (Chattopadhyay, 2024).

The objective of this study was to evaluate EMG-classification approaches that integrate preprocessing, feature extraction, and dimensionality reduction via principal component analysis. Raw EMG corresponding to seven hand movements was acquired and preprocessed, after which statistical features from the time, frequency, and time–frequency domains were computed. Classification was then performed using support vector machines (SVM) and artificial neural networks (ANN). The comparative analysis quantified the contribution of feature extraction and dimensionality reduction to overall performance and identified the more effective configuration between SVM and ANN.

2 Experimental Setup

2.1 Overview of the EMG processing workflow

Hand-movement classification was addressed via sequential processing stages, as summarized in Figure 1. First, surface electrodes are positioned over the forearm muscles that drive finger flexion, and single-channel EMG is acquired while the subject performs a set of predefined gestures. The raw recordings are then pre-processed to attenuate noise and artifacts and to obtain representations suitable for quantitative analysis.

In the second stage, each contraction is segmented and a set of handcrafted features is extracted from every segment. Time-domain, frequency-domain and time–frequency-domain descriptors are computed to characterize the amplitude, spectral content and joint time–frequency behavior of the EMG. These descriptors are concatenated into feature vectors.

Finally, dimensionality reduction is performed by Principal Component Analysis, and the resulting low-dimensional representations are used as input to supervised classifiers. In this work, support vector machines and artificial neural networks are trained on the reduced feature vectors to discriminate among the seven hand movements. The scatter plot in Figure 1 illustrates, schematically, how samples associated with different gestures are distributed in the reduced feature space.

2.2 Participants, gestures and acquisition hardware

Experiments were carried out with twelve healthy volunteers without known neuromuscular disorders. All participants were right-handed and performed the tasks with the dominant upper limb while seated comfortably, with the forearm supported to minimize gross motion. The study considered seven voluntary hand movements: global hand closing, flexion of each individual finger, and a pincer-type grasp in which the thumb approaches the remaining fingers.

Surface EMG was recorded using a MyoWare 2.0 sensor in differential configuration. Disposable Ag/AgCl electrodes were placed over the flexor muscle group of the forearm along the main fiber direction, and a reference electrode was attached to a bony region with minimal muscular activity. The analog output of the MyoWare module was connected to an STM32F407 development board, which provided analog-to-digital conversion and data logging to a host computer.

Signals were sampled at 5 kHz, which exceeds the bandwidth typically associated with surface EMG (approximately 20–500 Hz) and thus preserves the spectral content required for subsequent feature extraction. For each subject and gesture, a continuous recording of approximately 10 seconds was collected, yielding about 50 000 samples per trace at the chosen sampling rate.

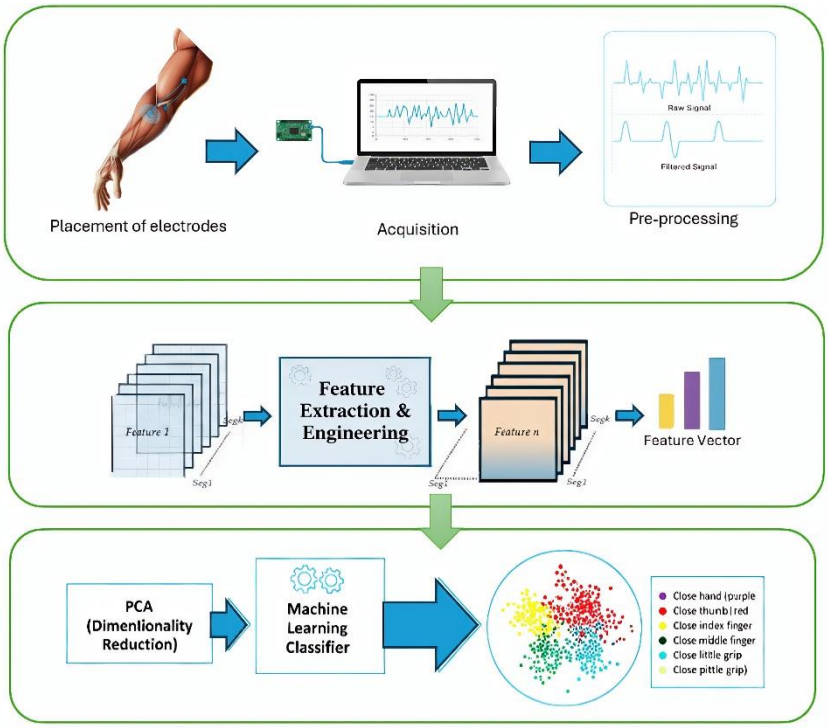

Figure 1. Schematic of the EMG-based hand-movement classification process. Surface EMG is acquired from forearm flexor muscles after electrode placement and pre-processed to obtain clean signals. From each contraction, time-, frequency- and time–frequency-domain features are extracted and assembled into feature vectors. Principal component analysis is then applied for dimensionality reduction, and the resulting low-dimensional representations are used to train machine-learning classifiers (SVM, ANN) to distinguish seven hand gestures.

2.3 Segmentation and dataset construction

To facilitate subsequent analysis, each EMG recording was divided into equal-length segments, as illustrated in Figure 2. For every trace, the desired number of segments was fixed to five, because each 10-s signal corresponds to five voluntary contractions executed by the subject during the trial. Knowing in advance the number of contractions makes it possible to design a segmentation procedure that consistently yields five segments per signal, ensuring a uniform structure across the dataset. In this way, each resulting segment captures a full contraction–relaxation cycle of the corresponding gesture, rather than arbitrary portions of the signal. Isolating each contraction delimitates the onset and offset of muscle activity and separates active and rest periods, which is important for computing features such as RMS, mean frequency and energy on windows that contain only task-relevant EMG. The approximate length of each segment was obtained by dividing the total number of samples in the recording by five and rounding the result to the nearest lower integer. This length was then used to cut the continuous EMG trace into contiguous, non-overlapping sections. Working with non-overlapping segments avoids redundancy between samples and simplifies the interpretation of the extracted features, since each segment is associated with a distinct contraction. When the product of the segment length and the desired number of segments did not exactly match the original signal length, the segment length was slightly adjusted so that the complete recording was covered and all segments had the same duration. This minor adjustment ensured that no part of the signal was discarded and that all five segments within a trial were perfectly aligned in terms of sample count. In this way, each 10-s EMG trace was converted into five smooth segments that together contain all samples of the original signal and preserve the temporal structure imposed by the experimental protocol.

Applying this procedure to all recordings resulted in a balanced dataset with five segments for each combination of subject and gesture, that is, 5 segments × 7 gestures × 12 subjects = 420 EMG segments, corresponding to 60 labeled segments per gesture class. This balanced design avoids class imbalance effects and guarantees that all seven movements are equally represented in the subsequent analyses. Each segment inherits the label of the gesture performed and the identifier of the subject, which allows both per-class performance and subject-wise behavior to be examined in later stages if required. Before feature extraction, each segment was linearly normalized using min–max scaling to map its amplitude values into the [0, 1] interval, thereby reducing inter-subject differences in signal magnitude. Such differences arise naturally from variations in electrode placement, skin impedance and individual muscle morphology. By normalizing each segment independently, the resulting features become more comparable across participants and recording sessions, and the classifiers can focus on differences in signal shape and temporal–spectral content rather than on absolute amplitude levels. The normalized segments constitute the input to the preprocessing, feature-extraction and PCA stages represented in Figure 2 and are ultimately used to train and evaluate the SVM and ANN classifiers described in Section 3.

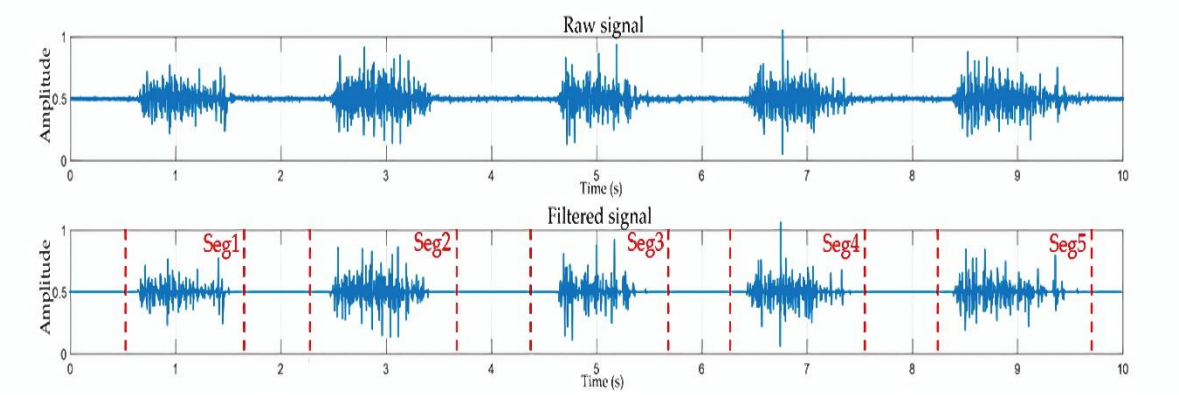

Figure 2. Example of EMG preprocessing and segmentation for a 10-s trial. From top to bottom: raw EMG, band-pass filtered EMG. The red dashed vertical lines indicate the boundaries of the five contiguous segments (Seg1–Seg5) obtained from the recording, each corresponding to a single voluntary contraction.

2.4 Hand gesture tasks

Before each recording session, the skin over the forearm flexor muscles was prepared to ensure good electrode–skin contact and to reduce impedance. The area was gently cleaned with an alcohol wipe to remove superficial oils and dead skin, and excess hair was trimmed when necessary. After the skin was dry, disposable Ag/AgCl electrodes were placed over the main flexor muscle group of the dominant forearm, following the same configuration described in Section 2.2. The reference electrode was attached to a bony region with minimal muscular activity. Once the electrodes and the MyoWare sensor were in place, signal quality was verified on screen while the participant performed a few test contractions, and the electrodes were adjusted if drift or excessive noise was observed.

Participants were seated comfortably in front of the recording setup, with the shoulder relaxed and the forearm resting on a support to minimize unwanted motion and reduce fatigue. During a short familiarization period, the experimenter explained the goal of the study and demonstrated each hand movement, using visual examples of the initial and final postures. The seven target gestures were shown on printed cards and on a monitor to ensure that all subjects used the same reference postures. Participants were instructed to reproduce the gestures "firmly but without discomfort", avoiding unnecessary co-contraction of other muscles and without moving the arm or shoulder. For each gesture, they were asked to open and close the hand or finger repeatedly for approximately 2 seconds per contraction, following verbal cues given by the experimenter. Each recording for a given gesture lasted about 10 seconds and contained a sequence of clearly identifiable contraction–relaxation cycles, which were later segmented as described in Section 2.3. Short rest pauses were included between gestures to avoid excessive fatigue and to keep signal quality stable throughout the session.

The protocol comprised seven voluntary movements, illustrated in Figure 3. In Test 1, the subject performed a global hand-closing gesture. Starting from a fully open hand with all fingers extended and separated, the participant closed all fingers simultaneously into a fist and then returned to the open position. This pattern was repeated several times during the 10-s trial and represents a compound movement that strongly activates the forearm flexor muscles. In Test 2, only the thumb was activated. The hand remained otherwise relaxed and open, while the thumb flexed towards the palm and then extended back to its initial position. This gesture isolates thumb activity, which is relevant for grasping tasks and typically generates a different activation pattern than multi-finger flexion. Test 3 isolated the index finger. Starting from the open-hand posture, the index finger was flexed and extended repeatedly while the remaining fingers and thumb stayed as relaxed as possible. The experimenter reminded participants to avoid moving other fingers to obtain a clearly distinguishable pattern associated with index-finger activation. In Test 4, the same pattern was followed for the middle finger, emphasizing its individual flexion and extension. Because independent control of this finger is sometimes more difficult, additional verbal feedback was provided when participants tended to move adjacent fingers. Test 5 targeted the ring finger. Participants were asked to focus on flexing only this finger while keeping the others extended. This task is intentionally more demanding from a motor-control perspective and was included to evaluate the classifier under conditions where selective activation is harder to achieve. Test 6 involved isolated flexion of the little finger. Again, the subject started from an open-hand posture, flexed the little finger towards the palm and then returned to the initial position after each contraction. This gesture completes the set of single-finger movements, covering all digits of the hand.

Finally, Test 7 corresponded to a pincer grip. The subject brought the thumb towards the fingertips to form a pinch, mimicking the action of grasping a small object between the thumb and the remaining four fingers, and then returned to the open-hand posture. This gesture was included because pincer grips are functionally important in daily activities and typically recruit a different combination of muscles compared with isolated finger flexion or global hand closing.

Across all tests, the same timing and recording conditions were maintained so that each 10-s trial contained approximately five contractions separated by short rest intervals. The order of the gestures followed the sequence shown in Figure 3 and was the same for all participants, which simplifies subsequent analysis and comparison across subjects. This standardized protocol ensured that the EMG data for the seven gestures were comparable across recordings and provided consistent input for the segmentation, feature-extraction and classification stages described in the following sections.

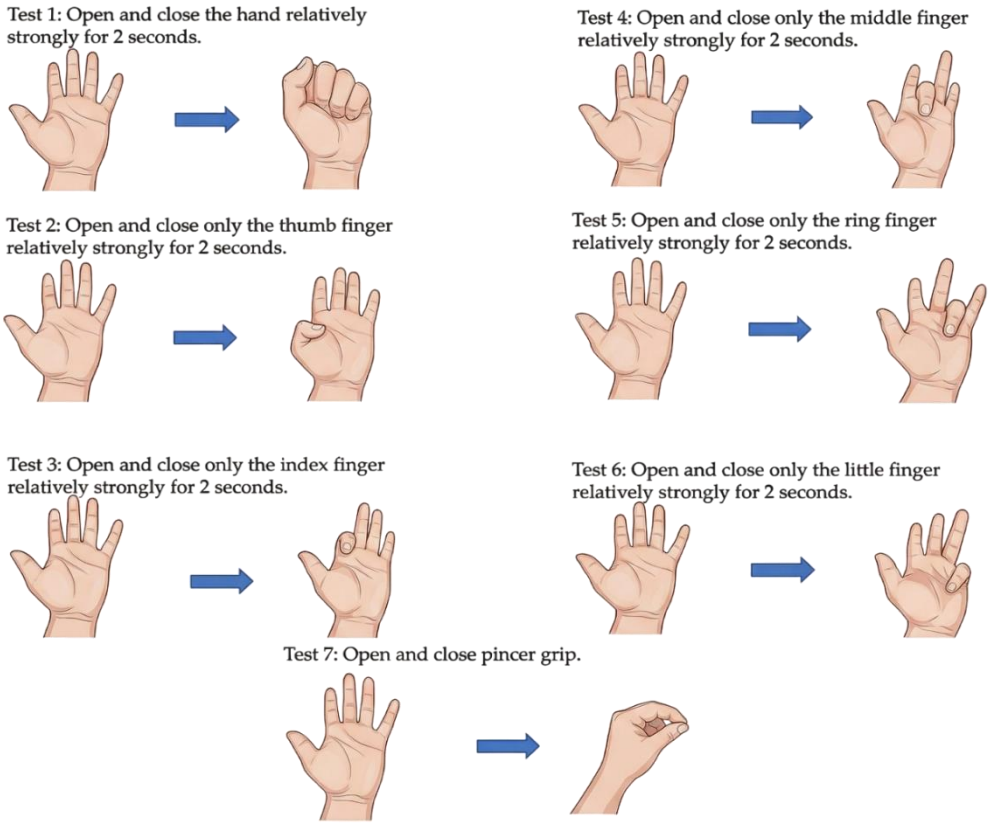

Figure 3. Hand-gesture tasks considered in the study. From Test 1 to Test 7: (1) repeated global hand closing, (2) isolated thumb flexion, (3) isolated index-finger flexion, (4) isolated middle-finger flexion, (5) isolated ring-finger flexion, (6) isolated little-finger flexion, and (7) pincer grip.

2.5 Feature extraction

Feature extraction is the step that transforms segmented EMG windows into quantitative descriptors that are suitable for classification. Instead of working directly with raw samples, a set of metrics is computed to summarize the most relevant characteristics of each segment, reducing data dimensionality while preserving information that is discriminative for hand-gesture recognition. In this work, features are computed in three domains: time, frequency and time–frequency.

Time-domain features capture how the amplitude of the signal evolves over the segment. Metrics such as Mean Absolute Value (MAV), Root Mean Square (RMS), skewness and related statistics describe the intensity, variability and symmetry of muscle activation. Frequency-domain features characterize how the signal energy is distributed across frequencies. Autoregressive (AR) coefficients, total spectral power and spectral entropy provide information about dominant frequency components and the overall complexity of the spectrum. Time–frequency features are obtained using a wavelet-based analysis, which decomposes the EMG into sub-bands with specific time and frequency localization. From these coefficients, wavelet energies and wavelet entropy are computed to capture transient and non-stationary behavior.

The complete set of 17 features used in this study is summarized in Table 1. Together, these temporals, spectral and time–frequency descriptors provide a compact yet informative representation of each EMG segment, balancing simplicity and discriminative power for subsequent classification of the seven hand gestures.

Table 1. Extracted EMG features across time, frequency, and time–frequency domains

Feature	Mathematical representation
MAV	$\frac{1}{N}\sum_{n=1}^{N} x[n]$
RMS	$\frac{1}{N}\sum_{n=1}^{N} x[n]^2$
Skewness	$\frac{1}{\sigma^3}\cdot\frac{1}{N}\sum_{n=1}^{N}(x[n]-\mu)^3$
Kurtosis	$\sigma^4\cdot\frac{1}{N}\sum_{n=1}^{N}(x[n]-\mu)^4$
Maximum Value	$\max(x[n])$
AR Coefficients AR_1 to AR_4	$\sum_{k=1}^{4} a_k x[n-k]+e[n]$
Total Spectral Power	$\sum_{k=1}^{p} a_k^2$
Spectral Entropy	$-\sum_{k} p_k \log(p_k),\ p_k=\frac{\sum_k P[k]}{P[k]}$
Spectral Kurtosis	$\sigma_P^4\sum_{k}\left(P[k]-\mu_P\right)^4$
Wavelet Energy (cD_1 to cD_4)	$E_{cD_i}=\sum_{n=1}^{M}\lvert cD_i[n]\rvert\ ;i\ =\ 1,2,3,4$
Wavelet Entropy cD_4	$H_{cD_4}=-\sum_{n} p_{cD_4}[n]\log\left(p_{cD_4}[n]\right)$ Where: $p_{cD_4}[n]=\frac{\lvert cD_4[n]\rvert}{\sum\lvert cD_4[n]\rvert}$

While time-domain metrics such as Waveform Length (WL), Zero Crossings (ZC), and Slope Sign Changes (SSC) are frequently utilized in EMG pattern recognition, they were excluded from this study to minimize feature redundancy and avoid the limitations of threshold-dependent descriptors. It has been demonstrated that ZC and SSC function as indirect estimates of frequency information and are highly sensitive to background noise levels, necessitating the calibration of heuristic amplitude thresholds to function correctly (Phinyomark et al., 2012). In contrast, the spectral properties of the signal were explicitly modeled in this work using Autoregressive (AR) Coefficients and Total Spectral Power, which provide a more robust representation of the frequency content without relying on subject-specific noise thresholds (Oskoei, M. A., & Hu, H. (2007). Furthermore, signal complexity was characterized through Spectral and Wavelet Entropies rather than Waveform Length; these information-theoretic measures effectively quantify the stochastic disorder of the myoelectric signal (Sharma et al., 2024), offering a superior generalization capability for non-stationary segments compared to geometric amplitude accumulations.

2.6 Feature engineering

In addition to the original 17 descriptors, a set of engineered features was created by applying simple mathematical transformations to selected time-, frequency- and time–frequency-domain metrics, Figure 4. The goal of this step is to enrich the representation of each EMG segment with nonlinear combinations that emphasize differences between gestures, mitigate skewness and stabilize variance, while keeping the individual transformations easy to interpret from a physiological and statistical standpoint. The transformations used in this study are summarized in Table 2.

A first group of transformations involves polynomial mappings of the original features. Squaring and cubing selected amplitude-related descriptors (for example RMS or MAV) amplify contrasts between low and high activation levels: segments with small values remain close to zero, whereas segments with larger values increase disproportionately. These nonlinear mappings can highlight subtle differences in muscle activation that might be less apparent when using only the original, linear scale.

A second group comprises root and logarithmic transformations, which have the opposite effect: they compress large values and spread out values near zero. Applying square-root and log mappings to positively valued features helps to reduce the influence of extreme outliers and to obtain distributions that are closer to symmetric. This is particularly useful for EMG descriptors that tend to be right-skewed, such as power- or energy-based measures.

We also considered ratio-type features that combine information from two complementary descriptors. The ratio between RMS and MAV, for instance, relates an energy-like measure to a mean amplitude and can be interpreted as a normalized indicator of variability. Similarly, the ratio between RMS and skewness links the overall magnitude of the signal to the asymmetry of its distribution. These composite quantities encode interactions that are not captured by each descriptor in isolation and can therefore provide additional discriminative cues to the classifier.

To couple spectral and time–frequency information, we constructed hybrid features that mix wavelet-based and spectral descriptors. One example is the combination of wavelet entropy from a specific detail level with a global spectral measure such as total spectral power or spectral entropy. The resulting indicators jointly reflect how concentrated the energy is in a particular sub-band and how complex the overall spectrum is. This is consistent with the non-stationary nature of EMG, where both local transients and global frequency content are relevant for distinguishing different hand gestures.

Finally, a Yeo–Johnson transformation was applied to selected features in order to further reduce skewness and stabilize variance. This family of power transformations is defined in such a way that it can handle both positive and negative values, making it suitable for descriptors that may cross zero. By tuning its shape parameter, the Yeo–Johnson transform can bring markedly non-Gaussian feature distributions closer to a symmetric, bell-shaped form.

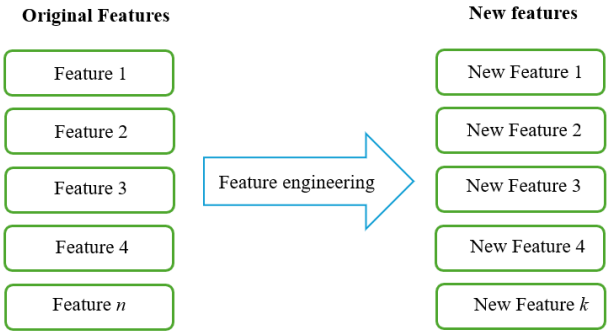

Figure 4. Schematic illustration of the feature-engineering step. Original EMG features are transformed through a set of mathematical operation.

3 Machine-Learning Classification Models

Once the EMG segments are represented by the extracted and engineered features, a supervised classifier is required to assign each sample to one of the seven hand-gesture classes. In this work, we focus on two widely used machine-learning models for bioelectrical signal analysis: support vector machines and artificial neural networks. Both approaches can model nonlinear decision boundaries in the feature space, but they do so in different ways. SVM constructs separating hyperplanes with maximum margin using kernel functions, whereas ANN learns a set of weighted connections organized in layers of neurons. By training and comparing these two classifier families on the same feature space, it is assessed how effectively each method exploits the information yielded by EMG feature extraction and the reduced representation.

3.1 Support Vector Machine

SVM was selected as one of the baseline models because it is widely used for EMG and biomedical classification problems and can handle nonlinear decision boundaries through kernel functions. Conceptually, SVM seeks a separating surface in the feature space that maximizes the margin between samples from different classes, which tends to improve generalization on unseen data.

In this study, SVM was applied to the PCA-transformed feature vectors obtained from the EMG segments. Three kernel types were considered: linear, radial basis function (RBF) and polynomial of degree three, as summarized in Table 2. The linear kernel provides a reference for purely linear separation in the reduced feature space. The RBF kernel allows flexible, locally adaptive decision boundaries by measuring similarity as a function of the distance between samples. The polynomial kernel introduces controlled nonlinear interactions between features through low-order polynomial terms.

Because the problem involves seven gesture classes, a one-vs-one strategy was adopted, in which a separate binary SVM is trained for each pair of classes and final labels are assigned by majority voting. For each kernel, the regularization parameter and kernel-specific hyperparameters (such as the RBF width and polynomial degree/offset) were tuned using grid search combined with cross-validation on the training set. This procedure ensures that the reported performance reflects configurations that are reasonably optimized for the proposed EMG feature space.

Table 2. SVM Kernel Functions

Kernel	Mathematical representation
Linear	$K(x, x') = x^\top x'$
RBF	$K(x, x') = \exp(-\gamma \lvert x - x' \rvert^2)$
Polynomial (grade = 3)	$K(x, x') = (x^\top x' + c)^d$

3.2 Artificial Neural Network

An ANN was also evaluated to classify the reduced feature vectors corresponding to the seven hand gestures. In this case, a multilayer perceptron was implemented with an input layer matching the dimensionality of the reduced feature space, three fully connected hidden layers with ReLU activations, and an output layer with seven neurons and softmax activation to perform multi-class classification.

The network was trained for 300 epochs using mini-batches of 64 samples and an initial learning rate of 1×10^{-4}. Batch normalization and dropout were included in the hidden layers in order to stabilize training and reduce overfitting. All weights and biases were updated with the Adam optimizer, minimizing categorical cross-entropy as the loss function.

This architecture follows configurations that have been frequently reported in recent EMG-classification studies and, in preliminary tests, offered a reasonable compromise between model capacity and generalization. A full hyperparameter search was not carried out due to computational constraints; however, the selected settings showed stable behavior and consistent performance across the different training runs considered in this work.

3.3 Principal Component Analysis

Dimensionality reduction was applied to the full set of extracted and engineered features prior to classification. The transformation was fitted using only the training data, and the resulting projection was then applied to both training and test sets to avoid information leakage. Three configurations were considered, retaining 2, 5, 9 and 12 principal components, respectively. These values were selected to analyze the effect of progressively increasing dimensionality: two components provide an extremely compact representation that is also convenient for visualization, five components offer an intermediate setting, and twelve components preserve a larger portion of the original variance while still reducing feature dimensionality. For each configuration, the PCA-transformed feature vectors were used as input to the SVM and ANN classifiers, and the corresponding results were compared.

4 Results

Table 4 summarizes the overall classification performance obtained when the classifiers were trained directly on the full set of extracted and engineered features, without applying PCA. Among the SVM configurations, the linear kernel achieved the highest accuracy (92.52%), closely followed by the polynomial kernel, while the RBF kernel yielded slightly lower values. ANN reached an accuracy of 89.52%, a few percentage points below the best SVM configurations. F1-score and recall showed the same pattern, with very similar values across metrics for each classifier, indicating a good balance between correctly detected gestures and the proportion of missed samples.

These results indicate that, in the original feature space (before dimensionality reduction), the seven hand-gesture classes are already reasonably well separated, so relatively simple decision boundaries are sufficient to discriminate them. The small difference between the linear and polynomial SVM suggests that additional nonlinear terms provide only marginal gains, whereas the RBF kernel does not bring further improvement under the current settings. Compared with ANN, SVM consistently attains higher accuracy, F1-score and recall in this baseline condition, and therefore serves as a strong reference point for the PCA-based experiments reported in the following subsections.

Table 4. Classification performance of SVM and ANN

	Algorithm	Accuracy (%)	F1-Score	Recall
SVM	Linear Kernel	92.52	0.9249	0.9252
	RBF Kernel	91.04	0.9097	0.9100
	Poly Kernel	92.47	0.9246	0.9247
	ANN	89.52	0.8937	0.8952

The confusion matrices in Figure 5(a–c) provide a detailed view of the class-wise behavior of the three SVM kernels without prior feature-space projection Classes 1–7 correspond respectively to ring finger (1), index finger (2), middle finger (3), little finger (4), thumb (5), full hand closing (6) and pincer grip (7). In the three matrices, the diagonal entries clearly dominate, which confirms that most segments are assigned to the correct gesture. Index, middle and thumb flexion (classes 2, 3 and 5) together with the pincer grip (class 7) exhibit the highest diagonal values, typically close to or above 87%, in agreement with the high global accuracy values reported in Table 4 for the linear and polynomial kernels.

Misclassifications concentrate mainly within the group of single-finger flexion gestures of the ring, middle and little fingers and between these gestures and full hand closing (class 6). For example, ring-finger segments (class 1) are often predicted as little finger (class 4) and, to a lesser extent, middle finger (class 3) or full hand closing, while little-finger segments (class 4) show confusions with ring finger and full hand closing. These error patterns are anatomically plausible, since these gestures recruit overlapping forearm flexor muscles. The RBF kernel tends to spread these errors more across neighboring classes, whereas the linear and polynomial kernels keep them more localized, which is consistent with their slightly better overall performance. Overall, the confusion matrices confirm that the main challenge lies in separating gestures with similar activation patterns, while gestures with more distinctive muscle recruitment, index, middle, thumb and pincer, are reliably recognized by all SVM configurations.

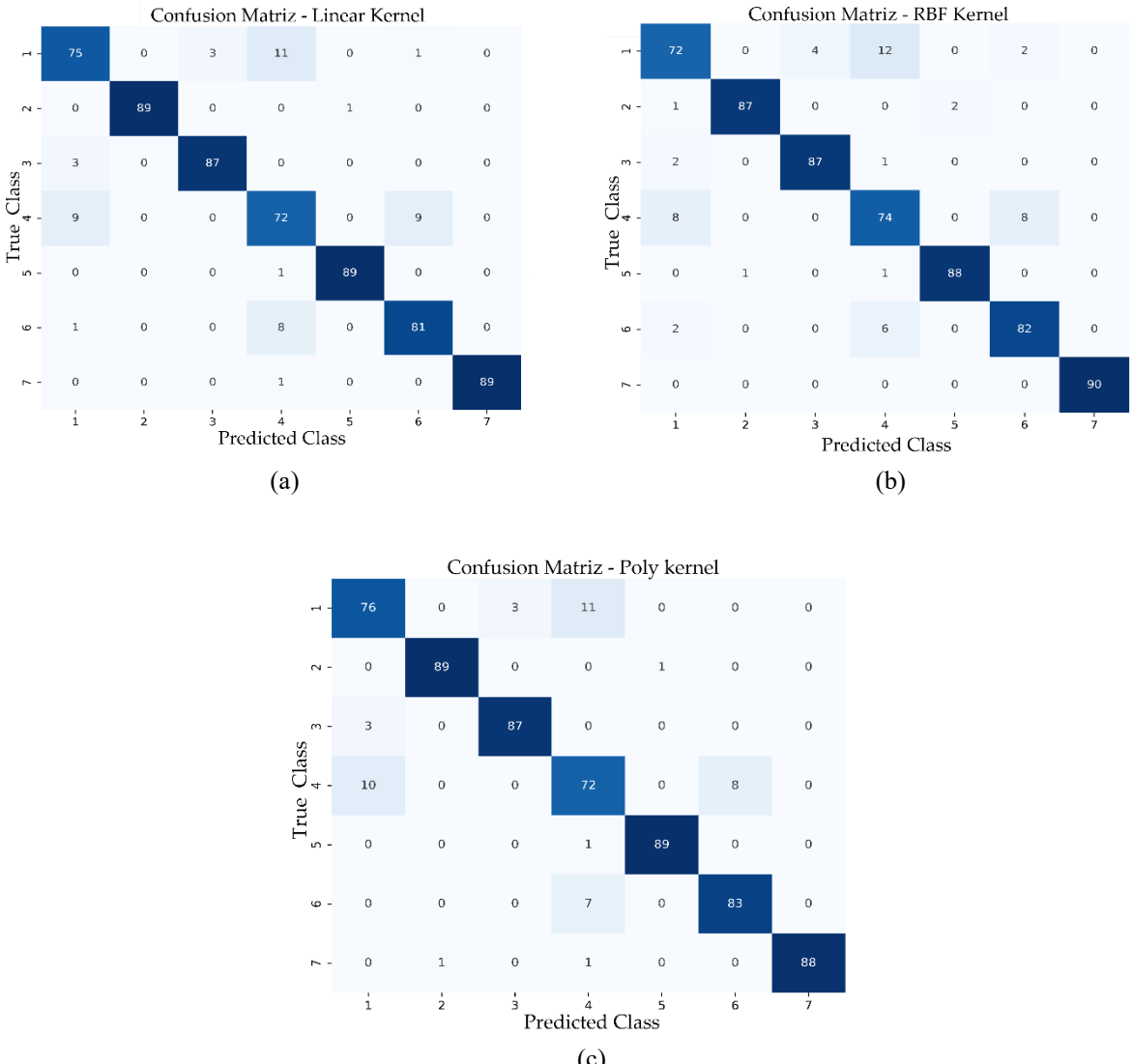

(a) (b) (c)

Figure 5. Confusion matrices for SVM classifiers trained on the original feature space (no PCA): (a) linear kernel, (b) RBF kernel, and (c) polynomial kernel.

The confusion matrix in Figure 6 summarizes the behavior of the ANN classifier in the same no-PCA condition reported in Table 4. Most of the mass is concentrated on the main diagonal, confirming that the network correctly identifies the majority of segments for each gesture. However, the off-diagonal entries are more pronounced than in the SVM matrices, particularly in the first and fourth rows, where a noticeable fraction of samples is exchanged between these two classes and, to a lesser extent, with the sixth class. In contrast, the remaining gestures show almost perfect recognition, with only a few isolated misclassifications. This pattern reveals that the ANN tends to perform very well for some gestures while struggling with a small subset of movements that elicited more similar EMG patterns.

This behavior is consistent with the global metrics in Table 4: although ANN attains a high overall accuracy close to 90%, its F1-score and recall remain lower than those of the best SVM configurations. The concentration of errors in a few specific gestures penalizes the average performance and leads to a less balanced class-wise behavior compared with SVM, whose confusion matrices exhibit more uniformly high diagonal values. In other words, the ANN is capable of modeling the separability present in the original feature space, but it is slightly less effective than SVM at handling subtle differences between gestures with overlapping muscle activation, which explains the performance gap observed in the baseline condition.

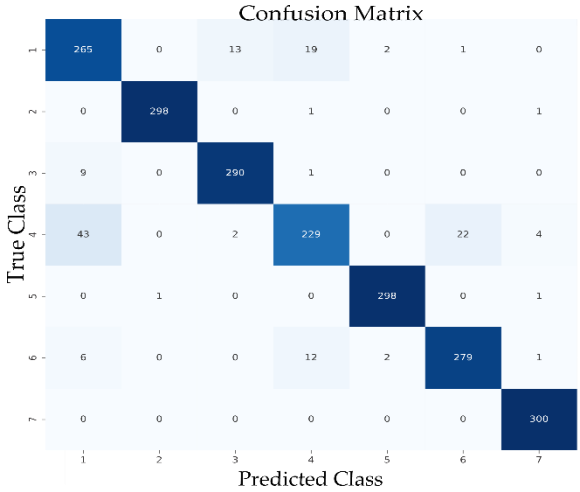

Figure 6. Confusion matrix for ANN on EMG hand-gesture classification, no PCA.

Misclassifications observed in the confusion matrices can be interpreted in light of forearm functional anatomy and the superposition of motor-unit activity captured by a single sEMG channel. Finger flexion is largely mediated by the flexor digitorum superficialis and flexor digitorum profundus, whose muscle compartments and tendinous architecture are partially shared across digits and are activated through coordinated neural drive. Consequently, neighboring fingers can produce highly similar activation patterns in the flexor compartment, particularly when common flexion synergies and comparable force levels are recruited. This similarity is expected to yield overlapping distributions of handcrafted features, thereby increasing confusion among gestures that differ only by the specific digit involved.

Classifier performance was assessed using the Friedman test applied to paired fold-wise accuracies obtained under the same stratified 5-fold cross-validation splits (SVM with linear, RBF, and polynomial kernels, and ANN). No statistically significant differences were detected among models in the no-PCA condition ($\chi^2 = 4.0625$, $p = 0.2548$; $\alpha = 0.05$). Accordingly, the differences observed in mean accuracy should be interpreted as non-conclusive from an inferential standpoint, and model selection can be guided by practical criteria such as simplicity and computational cost.

To assess the impact of PCA on classification performance, the feature set was projected onto subspaces spanned by two, five, nine and twelve principal components. These projections preserved approximately 64 %, 87 %, 95 % and 97 % of the total variance of the original features, respectively, which allows us to study how performance changes as a larger fraction of the original variance is retained. The corresponding metrics for each classifier and each dimensionality setting are reported in Tables 5–8.

For the linear SVM, the loss of information produced by aggressive dimensionality reduction is evident. When the input is reduced to two principal components, accuracy decreases to 70 %, more than twenty percentage points below the reference result obtained without dimensionality reduction, where the same classifier reaches 92.52 %. Increasing the number of components leads to a steady recovery: with five components the accuracy rises to 89.52 %, and with nine and twelve components the values reach 91.11

% and 91.59 %, respectively. Despite this improvement, even the best PCA configuration for the linear SVM remains slightly below the baseline without feature-space projection, and the same pattern appears in F1-score and recall. These observations indicate that the linear classifier already exploits the structure of the original feature space efficiently; projecting onto a smaller set of principal directions removes information that is still useful for defining the decision boundaries.

The polynomial SVM is even more sensitive to dimensionality reduction. With only two components, accuracy falls to 65.24 %, which represents a severe degradation compared with the 92.47 % obtained in the original feature space. When five components are retained, accuracy improves to 85.87 %, and for nine and twelve components the values increase further to 87.46 % and 87.62 %. However, all these configurations remain clearly below the no-PCA baseline, with differences of around four to five percentage points in accuracy and similar gaps in F1-score and recall. This suggests that the polynomial kernel relies on more subtle interactions among the original features, and that these interactions are only partially preserved after projection onto the principal-component subspace.

The behavior of the RBF SVM is qualitatively different. With two components, accuracy is still limited to 73.17 %, reflecting the loss of discriminative structure when only about two thirds of the total variance is maintained. Once five components are used, the model almost recovers its original performance, achieving an accuracy of 91.11 %, which is essentially comparable to the 91.04 % obtained prior to dimensionality reduction. When nine and twelve components are retained, accuracy rises to 91.90 % and 92.54 %, respectively, and both F1-score and recall show the same monotonic improvement. In this case, projecting onto a moderately reduced subspace that preserves more than 94 % of the variance appears to filter out noise and redundancy in the feature set, leading to a slight but consistent gain in generalization capability relative to the baseline.

The ANN benefits the most from PCA. When only two principal components are provided as input, accuracy remains at 69.29 %, which is markedly lower than the 89.52 % obtained without dimensionality reduction. Retaining five components already suffices to recover the baseline, with an accuracy of 89.76 %. When the dimensionality is increased to nine components, accuracy improves to 93.10 %, and with twelve components it reaches 93.81 %. In this higher-variance regime the network outperforms not only its own configuration without applying principal-component reduction but also all SVM variants, with gains of approximately three to four percentage points in accuracy, F1-score and recall. This indicates that the neural network clearly benefits from receiving a compact, decorrelated representation that concentrates the most informative variance of the original feature set.

Table 5. Performance of linear SVM with PCA

Component	Variance explained (%)	Accuracy (%)	F1-Score	Recall
2	64.2429	70.0000	0.6998	0.7000
5	87.0224	89.5238	0.8955	0.8952
9	94.5797	91.1111	0.9111	0.9111
12	96.8891	91.5873	0.9161	0.9158

Table 6. Performance of RBF SVM with PCA

Component	Variance explained (%)	Accuracy (%)	F1-Score	Recall
2	64.2429	73.1746	0.7333	0.7317
5	87.0224	91.1111	0.9110	0.9111
9	94.5797	91.9048	0.9185	0.9190
12	96.8891	92.5397	0.9254	0.9253

Table 7. Performance of polynomial SVM with PCA

Component	Variance explained (%)	Accuracy (%)	F1-Score	Recall
2	64.2429	65.2381	0.6515	0.6523
5	87.0224	85.8730	0.8659	0.8587
9	94.5797	87.4603	0.8811	0.8746
12	96.8891	87.6190	0.8828	0.8761

Table 8. Performance of ANN with PCA

Component	Variance explained (%)	Accuracy (%)	F1-Score	Recall
2	64.2429	69.2857	0.6962	0.6928
5	87.0224	89.7619	0.8968	0.8976
9	94.5797	93.0952	0.9305	0.9309
12	96.8891	93.8095	0.9377	0.9380

4 Conclusions

This work examined EMG-based hand-gesture classification using a single forearm channel and a processing framework combining segmentation, handcrafted features from the time, frequency and time–frequency domains, feature engineering and dimensionality reduction. Signals corresponding to seven gestures were acquired from twelve participants, segmented into contraction-level windows and described by a compact set of 17 primary features and additional engineered descriptors. These representations were then used to train SVM models with linear, RBF and polynomial kernels, as well as a multilayer perceptron, and the influence of PCA on classification performance was systematically evaluated.

Without dimensionality reduction, the best results were obtained with linear and polynomial SVM, which achieved accuracies slightly above 92 %, while the RBF kernel reached about 91 % and the ANN approximately 89.5 %. Confusion-matrix analysis showed that most errors occurred among gestures that recruit similar forearm flexor muscles, whereas gestures with more distinctive muscle activation patterns were reliably recognized. These findings indicate that, even with a single EMG channel and a moderate number of handcrafted features, classical machine-learning techniques can separate seven finger-related gestures with high accuracy.

PCA altered this picture in a controlled way. When the feature space was compressed too aggressively to two principal components, all classifiers suffered a marked degradation, confirming that such a low-dimensional projection removes essential discriminative information. Once five or more components were retained, corresponding to at least 87 % of the total variance, performance approached or exceeded the baseline obtained using uncompressed features. Linear and polynomial SVM remained slightly below their original accuracy after dimensionality reduction, suggesting that these models already exploit the structure of the full feature space efficiently. In contrast, the RBF SVM achieved a modest improvement when operating on PCA-reduced features, and the ANN obtained the largest benefit: with nine to twelve components, the neural network surpassed all SVM configurations, reaching accuracies close to 94 % together with consistently high F1-score and recall. This indicates that PCA can act as an effective denoising and decorrelation step for more flexible, high-capacity models.

Several limitations should be acknowledged. The database involved a relatively small number of subjects and a single acquisition channel, and only seven discrete gestures were considered. The classifiers were evaluated in an offline setting and only standard performance metrics were analyzed. Given the intended use in myoelectric-control scenarios, the computational cost of the overall processing stages is a relevant consideration. Feature extraction was based on windowed operations that are generally lightweight: most time-domain statistics are obtained by a single pass through the samples in each window, spectral descriptors are computed from an FFT-based power spectrum, and wavelet-based time–frequency features can be implemented efficiently through standard filter-bank operations. Once the PCA projection is learned offline, its online use reduces to a simple linear projection of the feature vector, which typically adds negligible overhead. Classification is also computationally manageable for linear and polynomial SVMs and for small multilayer perceptrons, whereas kernel SVMs remain feasible when the number of support vectors is moderate. Therefore, under standard EMG windowing and update rates used in control, near-real-time execution on embedded platforms is expected to be feasible with the proposed method (ARM-class processors), although device-level measurements of end-to-end latency and power consumption were outside the scope of this study. Future work will extend the protocol to a larger and more diverse cohort of participants and a richer gesture set, as well as real-time experiments. Additional studies will explore alternative feature sets, other dimensionality-reduction strategies and more advanced models, including ensemble methods and deep architectures, with the aim of improving robustness and generalization while preserving the low computational cost required for myoelectric-control applications.

Notwithstanding the high within-subject accuracies reported here, the present evaluation was subject-dependent, consequently, the metrics may overestimate performance on unseen users. While absolute accuracies are expected to decrease under LOSO, the relative ranking between SVM and ANN and the observed PCA effects are anticipated to remain consistent. Future work will adopt subject-independent protocols (e.g., leave-one-subject-out, LOSO) with leakage-safe preprocessing, i.e., scaling and PCA fitting restricted to the training subjects, to quantify cross-user generalization.

References

Alhatemi, R. A. J., & Savaş, S. (2024). A weighted ensemble approach with multiple pre-trained deep learning models for classification of stroke. *Medinformatics, 1*(1), 10–19. https://doi.org/10.47852/bonviewMEDIN32021963

Anam, K., Ismail, H., Hanggara, F. S., Avian, C., & Worsito, S. B. (2021). Cross validation configuration on k-NN for finger movements using EMG signals. In *2021 7th International Conference on Instrumentation, Control, and Automation (ICA)* (pp. 17–21). IEEE. https://doi.org/10.1109/ICA52848.2021.9625699

Asghari Oskoei, M., & Hu, H. (2007). Myoelectric control systems—A survey. *Biomedical Signal Processing and Control, 2*(4), 275–294. https://doi.org/10.1016/j.bspc.2007.07.009

Chattopadhyay, S. (2024). Towards predicting recurrence risk of differentiated thyroid cancer with a hybrid machine learning model. *Medinformatics*. Advance online publication. https://doi.org/10.47852/bonviewMEDIN42024441

Chen, C., Yu, Y., Sheng, X., Meng, J., & Zhu, X. (2023). Real-time hand gesture recognition by decoding motor unit discharges across multiple motor tasks from surface electromyography. *IEEE Transactions on Biomedical Engineering, 70*(7), 2058–2068. https://doi.org/10.1109/TBME.2023.3234642

Chen, Z., Min, H., Wang, D., Xia, Z., Sun, F., & Fang, B. (2023). A Review of Myoelectric Control for Prosthetic Hand Manipulation. *Biomimetics, 8*(3), Article 328. https://doi.org/10.3390/biomimetics8030328

Coskun, M., Yildirim, O., Demir, Y., & Acharya, U. R. (2022). Efficient deep neural network model for classification of grasp types using sEMG signals. *Journal of Ambient Intelligence and Humanized Computing, 13*(9), 4437–4450. https://doi.org/10.1007/s12652-021-03284-9

Joshi, M., & Singh, B. K. (2024). Deep learning techniques for brain lesion classification using various MRI (from 2010 to 2022): Review and challenges. *Medinformatics*. Advance online publication. https://doi.org/10.47852/bonviewMEDIN42021686

Khan, S. M., Khan, A. A., & Farooq, O. (2021). Pattern recognition of EMG signals for low level grip force classification. *Biomedical Physics & Engineering Express, 7*(6), Article 065012. https://doi.org/10.1088/2057-1976/ac2354

Lee, K. H., Min, J. Y., & Byun, S. (2022). Electromyogram-based classification of hand and finger gestures using artificial neural networks. *Sensors, 22*(1), Article 225. https://doi.org/10.3390/s22010225

Li, Y., Huang, Y., & Zhao, Q. (2022). Real-time collection and analysis of sports index time series based on multimodal sensor monitoring. *Journal of Sensors, 2022*, Article 7244856. https://doi.org/10.1155/2022/7244856

Lv, J., Yang, Y., Niu, L., Sun, X., Wang, L., Lin, W., Rong, H., & Zou, L. (2023). Prediction of hand grip strength based on surface electromyographic signals. *Journal of King Saud University - Computer and Information Sciences, 35*(5), Article 101548. https://doi.org/10.1016/j.jksuci.2023.04.001

Narayan, Y. (2021). Comparative analysis of SVM and Naive Bayes classifier for the SEMG signal classification. *Materials Today: Proceedings, 37*, 3241–3245. https://doi.org/10.1016/j.matpr.2020.09.093

Phinyomark, A., Phukpattaranont, P., & Limsakul, C. (2012). Feature reduction and selection for EMG signal classification. *Expert Systems with Applications, 39*(8), 7420–7431. https://doi.org/10.1016/j.eswa.2012.01.102

Rasnayake, R. M. P. K., Maduranga, M. W. P., & Sithara, J. P. D. M. (2022). Surface electromyography signal acquisition and classification using artificial neural networks (ANN). *International Journal of Modern Education and Computer Science, 14*(3), 64–75. https://doi.org/10.5815/ijmecs.2022.03.04

Sharma, A., Sharma, I., & Kumar, A. (2024). Signal acquisition and time-frequency perspective of EMG signal-based systems and applications. *IETE Technical Review, 41*(4), 466–485. https://doi.org/10.1080/02564602.2023.2265897

Subasi, A., & Qaisar, S. M. (2022). Surface EMG signal classification using TQWT, bagging and boosting for hand movement recognition. *Journal of Ambient Intelligence and Humanized Computing, 13*(7), 3539–3554. https://doi.org/10.1007/s12652-020-01980-6

Sun, B., Song, B., Lv, J., Chen, P., Sun, X., Ma, C., & Gao, Z. (2023). A multiscale feature extraction network based on channel-spatial attention for electromyographic signal classification. *IEEE Transactions on Cognitive and Developmental Systems, 15*(2), 591–601. https://doi.org/10.1109/TCDS.2022.3167042

Tepe, C., & Demir, M. C. (2022). Real-time classification of EMG Myo armband data using support vector machine. *IRBM, 43*(4), 300–308. https://doi.org/10.1016/j.irbm.2022.06.001

Unanyan, N. N., & Belov, A. A. (2021). Design of upper limb prosthesis using real-time motion detection method based on EMG signal processing. *Biomedical Signal Processing and Control, 70*, Article 103062. https://doi.org/10.1016/j.bspc.2021.103062

Zheng, Z., Wu, Z., Zhao, R., Ni, Y., Jing, X., & Gao, S. (2022). A review of EMG-, FMG-, and EIT-based biosensors and relevant human–machine interactivities and biomedical applications. *Biosensors, 12*(7), Article 516. https://doi.org/10.3390/bios12070516